

# DISCRETE RÖSSLER OSCILLATORS: MAPS AND THEIR ENSEMBLES

A.P. Kuznetsov<sup>a</sup>, Yu.V. Sedova<sup>a</sup>, N.V. Stankevich<sup>a,b</sup>

<sup>a</sup>Kotel'nikov's Institute of Radio-Engineering and Electronics of Russian Academy of Sciences, Saratov Branch  
Zelenaya 38, Saratov, 410019, Russian Federation  
apkuz@rambler.ru

<sup>b</sup>Laboratory of Topological Methods in Dynamics, National Research University Higher School of Economics,  
Bolshaya Pecherskaya str., 25/12, Nizhny Novgorod 603155, Russian Federation  
stankevichnv@mail.ru

## Abstract

We study the complex dynamics of a discrete analogue of the classical flow dynamical system - Rössler oscillator. Minimal ensembles of two and three coupled discrete oscillators with different topologies are considered. As the main research tool we used the method of Lyapunov exponents charts. For coupled systems, the possibility of two-, three- and four-frequency quasi-periodicity is revealed. Illustrations in the form of Fourier spectra are presented. Doublings of invariant curves, two- and three-dimensional tori are found. The transition from two-dimensional tori to three-dimensional ones occurs through a quasi-periodic saddle-node bifurcation of invariant tori or through a quasi-periodic Hopf bifurcation. A discrete version of the hyperchaotic Rössler oscillator is also discussed. It exhibits dynamical behavior close to a flow system in some measure.

Keywords: Rössler system, discrete map, Lyapunov exponent, quasi-periodicity, chaos, hyperchaos

# 1 Introduction

As we well know, two classes of dynamical systems are distinguished: continuous that described by differential equations (flows) and discrete described by iteration equations (maps). Maps arise at the study of a flow system by the method of Poincaré sections, mainly in numerical analysis. For certain systems they can be built from the initial principles, for example, in the case of an impulsive action on the system [1]. However, another method is possible, which goes back to the first studies in the field of nonlinear dynamics. It consists in the discretization of differential equations by replacing time derivatives with finite differences [2-4]. The resulting model can be considered as an independent dynamical system. Generally, its dynamics is more complex and diverse than the dynamics of prototype flow system, although it inherits some of its properties. For example, a map can be non-invertible, and even for one-dimensional map chaos can occur; 2D map can demonstrate hyperchaos and singular Shilnikov discrete attractors [5]. Besides, an additional control parameter as the discretization step appears. Moreover, maps are much easier to study than flows. We should remark that at considering the results of numerical simulation, we also deal with a certain map, because numerical integration is a discretization with high accuracy. A similar situation can be in physical experiments, when as a result of measurements we have got discrete time series. In recent papers [5-7] one can see the results for maps of simulated neuron behavior, which can generate time series typical for neuron flow model, and for experimental time series. Another area where discretized flows can be useful is the implementation of a system on microcontrollers. Microcontrollers work with recursively specified memory cells, so a simple discrete model is needed to program an flow dynamical system to FPGA [8,9]. That is why it is important to investigate discretized flow dynamical systems.

Discretization allows us to introduce a variety of interesting examples. So this procedure can be subjected to equations of realistic systems. For example, discrete versions of predator-prey population dynamics [10], the simplest gene networks [11,12], the Lorentz-84 climate model [13], the Kislov-Dmitriev radiophysical generator [14], an autonomous generator of quasi-periodic oscillations [15] were constructed and studied. Not only realistic systems can be discretized, but also basic models of the oscillation theory and nonlinear dynamics. Thus, discrete versions of a nonlinear pendulum [2], a van der Pol oscillator [16,17], a hard-excited autogenerator [18], Bogdanov oscilla-

tor (a standard model with Bogdanov-Takens bifurcation) [19,20], a system of coupled phase oscillators (Kuramoto model) with a different number of oscillators [21-25] were considered. In this context, it is logical to consider another basic system of nonlinear dynamics - the Rössler system [26]. This is the subject of the present paper. Combining such models into some networks or chains can provide new opportunities for studying phenomena of synchronization and conditions for complicating dynamics [27,28]. Note that a preliminary study of the discrete Rössler oscillator was carried out in Ref. [29]. Here we will develop and supplement the corresponding results. We consider both the traditional version of the three-dimensional Rössler system [26] and its four-dimensional version [30], which demonstrates hyperchaos.

The paper is structured as follows. In Section 2 we examine three-dimensional discrete Rössler system. We shortly describe principle of discretization of flow systems and study dynamical regimes characteristic for this model. Then we consider ensembles of two and three coupled discrete Rössler oscillators. For three coupled systems we investigate the features of dynamical regimes picture depending on the coupling topology: chain vs ring. In Section 3 we present the results obtained for discrete hyperchaotic Rössler system. In Section 4 we provide main results and conclusions.

## 2 Three-dimensional Rössler system

### 2.1 Individual discrete oscillator

The classical Rössler system has the following form [26]

$$\begin{aligned}\dot{x} &= -y - z, \\ \dot{y} &= x + ay, \\ \dot{z} &= b + (x - r)z.\end{aligned}\tag{1}$$

Here  $x$ ,  $y$ ,  $z$  are dynamical variables,  $a$ ,  $b$ ,  $r$  are parameters. Let us apply the discretization procedure to system (1), i.e., we replace the corresponding derivatives with finite differences

$$\frac{dx}{dt} \rightarrow \frac{x_{n+1} - x_n}{\varepsilon}, \quad \frac{dy}{dt} \rightarrow \frac{y_{n+1} - y_n}{\varepsilon}, \quad \frac{dz}{dt} \rightarrow \frac{z_{n+1} - z_n}{\varepsilon},\tag{2}$$

where  $\varepsilon$  is the discretization parameter. We obtain the following map, namely

a discrete Rössler oscillator:

$$\begin{aligned}x_{n+1} &= x_n - \varepsilon(y_n + z_n), \\y_{n+1} &= y_n + \varepsilon(x_n + ay_n), \\z_{n+1} &= z_n + \varepsilon b + \varepsilon(x_n - r)z_n.\end{aligned}\tag{3}$$

Figure 1 shows a Lyapunov exponents chart of the system (3) on the plane of the parameters of the Rössler system  $(a, r)$  for a fixed value of the third parameter  $b = 0.2$ . Lyapunov exponents  $\Lambda$  were calculated using standard algorithms proposed in [31] and Gram-Schmidt orthogonalization. We consider trajectories of length  $10^5$  time units. To construct a chart of Lyapunov exponents, we take a threshold for determining zero, for  $|\Lambda| < \Theta$  we assume that it is equal to zero. For our numerical experiment, the threshold was fixed at  $\Theta = 10^{-4}$ . The cases of a relatively small discretization parameter  $\varepsilon = 0.1$  (*a*) and its large value  $\varepsilon = 1$  (*b*) are presented. The type of regime was determined by the spectrum of Lyapunov exponents  $\Lambda_i$ :

- P means a stable fixed point or periodic regime (all exponents are negative  $\Lambda_{1,2,3} < 0$ ),
- 2T means a closed invariant curve - a two-frequency quasi-periodic regime (one zero exponent  $\Lambda_1 = 0$ ,  $\Lambda_{2,3} < 0$ ),
- C means a chaos (one exponent is positive  $\Lambda_1 > 0$ ,  $\Lambda_{2,3} < 0$ ),
- H means a hyperchaos (two positive exponents  $\Lambda_{1,2} > 0$ ,  $\Lambda_3 < 0$ ),
- D means escape of trajectories to infinity.

Note that in continuous-time systems, two-frequency quasi-periodicity is associated with an invariant torus, the Poincaré section of which is an invariant curve. Therefore, for discrete maps the invariant curve regime is sometimes called a torus, see for example [32,33]. Such a regime can also be called a two-frequency torus in accordance with the number of incommensurable frequencies.

It can be seen that for a small value of the discretization parameter, both periodic and quasi-periodic regimes are possible in the system. In this case, the region of quasi-periodic dynamics is quite homogeneous: windows of resonant periodic regimes are not visually observed. For large values of the parameter  $\varepsilon$  in the area of quasi-periodic dynamics, one can see a conspicuous structure of Arnold's tongues (Fig. 1b).

Figure 2 shows examples of phase portraits of the discrete Rössler oscillator. In case (*a*), one can see a closed invariant curve (a two-frequency torus). As the parameter  $a$  increases, this curve undergoes a period-doubling bifurcation (*b*). Then the invariant curve loses its smoothness (*c*) and chaos

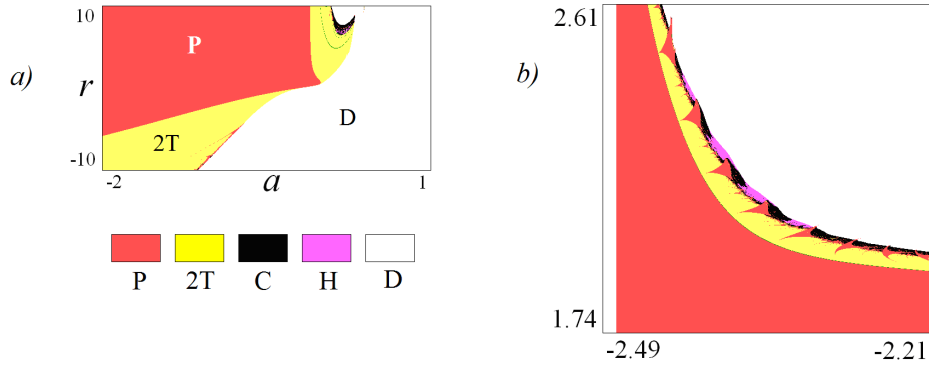


Figure 1: Lyapunov exponents chart of the discrete Rössler oscillator (3) for  $b = 0.2$ ;  $\varepsilon = 0.1$  (a) and  $\varepsilon = 1$  (b).

arises ( $d, e, f$ ). For convenience, next to each Figure, the value of the largest Lyapunov exponent  $\Lambda_1$  is indicated.

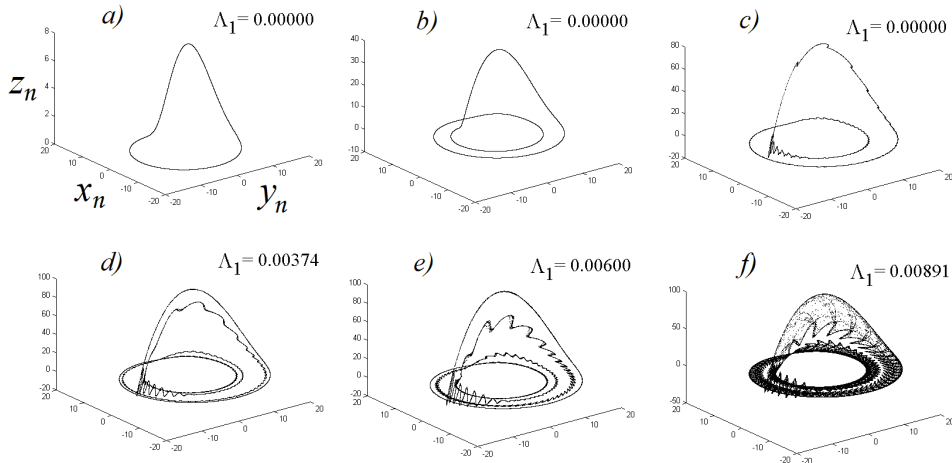


Figure 2: Attractors of the discrete Rössler oscillator,  $r = 9$ ,  $b = 0.2$ ,  $\varepsilon = 0.1$ . Values of parameters  $a$  are: (a)  $a = -0.02$ , (b)  $a = 0.04$ , (c)  $a = 0.0946$ , (d)  $a = 0.0976$ , (e)  $a = 0.1017$ , (f)  $a = 0.1042$ . The value of the largest Lyapunov exponent  $\Lambda_1$  is indicated.

The constructed system is a three-dimensional map. General properties of such discrete models are discussed in Ref. [34]. Note that such maps attract

attention in the context of the possibility of various types of chaotic attractors and doubling bifurcations of invariant curve [35-40]. At the same time, a three-dimensional generalization of the Hénon map is mainly investigated. Therefore, it is useful to replenish the collection of three-dimensional maps.

## 2.2 Two coupled discrete oscillators

Consider now two coupled discrete Rössler oscillators. Let us introduce the coupling between them by analogy with the continuous model [41-44]:

$$\begin{aligned}
x_{n+1} &= x_n - \varepsilon(y_n + z_n), \\
y_{n+1} &= y_n + \varepsilon(x_n + a_1 y_n) + \varepsilon\mu(v_n - y_n), \\
z_{n+1} &= z_n + \varepsilon b + \varepsilon(x_n - r)z_n, \\
u_{n+1} &= u_n - \varepsilon(v_n + w_n), \\
v_{n+1} &= v_n + \varepsilon(u_n + a_2 v_n) + \varepsilon\mu(y_n - v_n), \\
w_{n+1} &= w_n + \varepsilon b + \varepsilon(u_n - r)w_n.
\end{aligned} \tag{4}$$

Here  $\mu$  is the coupling parameter. Let us examine the structure of the control parameters plane  $(a_1, a_2)$  for subsystems. Figure 3 shows corresponding charts of Lyapunov exponents for two coupled systems (4) for different values of the discretization parameter  $\varepsilon$  and fixed coupling parameter  $\mu = 0.03$ . In the charts we designate new type of dynamical regime:

- 3T means an invariant 2D torus - a three-frequency quasi-periodic regime (two zero exponents  $\Lambda_1 = \Lambda_2 = 0$ ,  $\Lambda_{3,4,5,6} < 0$ ). In accordance with the number of incommensurable frequencies, this mode can also be called a three-frequency torus.

In Figure 3a the ranges of control parameters  $a_1$  and  $a_2$  are chosen in such a way that it corresponds to the transition in an individual oscillator from a stable fixed point to an invariant curve via Neimark-Sacker bifurcation, its subsequent doublings and destruction. Note that the resulting chart of regimes (Fig. 3) is symmetric with respect to the diagonal  $a_1 = a_2$ , since system (4) is symmetric with respect to the replacement of oscillators.

Let us first consider the case when discretization parameter  $\varepsilon$  is small (Fig. 3a). When moving on the parameter plane along the left and bottom edges of the chart in Fig. 3a one can detect a bifurcation scenario typical for a single model: birth of invariant curve from a fixed point via Neimark-Sacker bifurcation NS with its subsequent doublings and transition to chaos. In this case, the doubling line of invariant curve is fixed as a thin blue line,

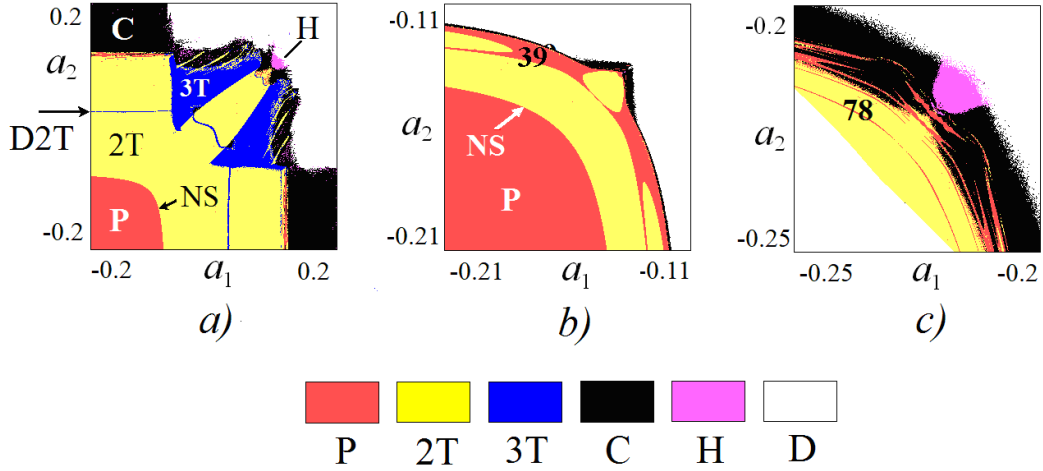


Figure 3: Lyapunov charts of two coupled discrete Rössler oscillators (4). Parameter values are  $r = 8.5$ ,  $b = 0.1$ ,  $\mu = 0.03$ ;  $\varepsilon = 0.1$  (a),  $\varepsilon = 0.16$  (b),  $\varepsilon = 0.2355$  (c).

since for this bifurcation two Lyapunov exponents vanish  $\Lambda_1 = \Lambda_2 = 0$ . The doubling line of two-frequency tori is marked with an arrow and denoted as D2T. Moreover, invariant curves and their doublings are possible in a neighborhood of the diagonal  $a_1 = a_2$ , on which the interacting subsystems are identical. In this area for enough big values of parameters we can see formation of hyperchaos.

As we mentioned above, for two coupled oscillators it is possible to observe a new type of dynamical regimes - three-frequency quasi-periodic regime 3T, characterized by two zero Lyapunov exponents  $\Lambda_{1,2} = 0$ ,  $\Lambda_{3,4,5,6} < 0$  and marked by blue color in Fig. 3a. Such a regime in the phase space is represented by an attractor in form of a two-dimensional torus. Note that the realization of 2D-tori requires some non-identity of subsystems with respect to the control parameters  $a_1$  and  $a_2$ . In this case, doubling of 2D-tori turns out to be possible, which is illustrated by the phase portraits in the projection onto the variables of the second oscillator in Figs. 4a and 4b. Phase portraits do not allow one to clearly visualize the torus doubling bifurcation. For this purpose, we construct cross-sections of phase portraits. Since model (4) is discrete, we cannot realize a cross-section, but we can fix a plane and consider points in some slice near this plane. By analogy with flow dynamical systems,

it will correspond to a map in the double Poincaré section [22,45]. Figures 4c and 4d show a cross-sections of the phase portraits (demonstrated on Fig. 4a and 4b respectively) by the plane  $v_n = -3$  and a slice near this plane  $|v_n + 3| < 10^{-2}$  with an additional condition  $u_n > 0$  to take into account the direction of rotation of the trajectory. In Fig. 4c, we can clearly detect an invariant curve, which is doubled in Fig. 4d. In both cases, these are smooth closed invariant curves. The doubling line of two-dimensional tori in Fig. 3a is a continuation of the D2T line in the 3T region.

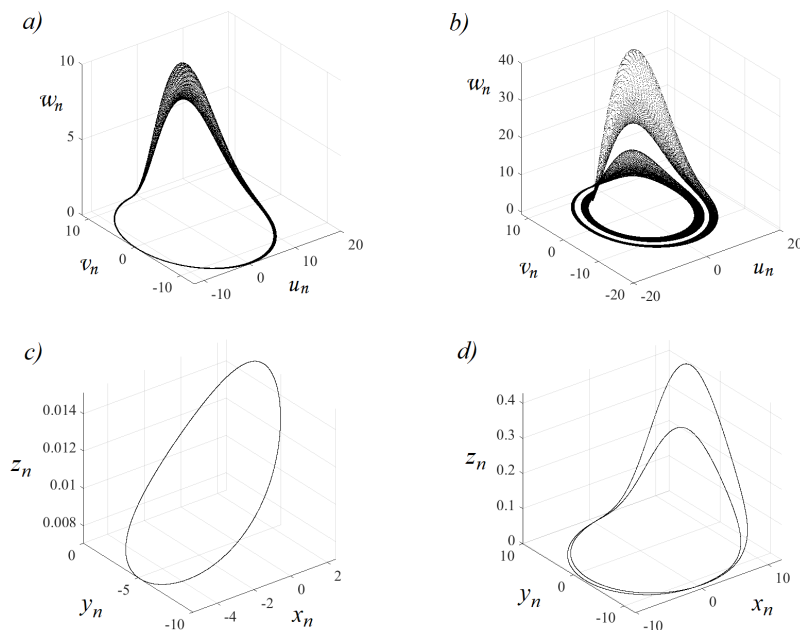


Figure 4: Two-dimensional (three-frequency) torus and its doubling in system of two coupled discrete Rössler oscillators (4) in phase portraits (top row) and their sections (bottom row),  $r = 8.5$ ,  $b = 0.1$ ,  $\mu = 0.03$ ,  $\varepsilon = 0.1$ . Control parameter values:  $a_1 = -0.06$ ,  $a_2 = 0.01$  ( $a, c$ ) and  $a_1 = -0.045$ ,  $a_2 = 0.05$  ( $b, d$ ).

As the discretization parameter  $\varepsilon$  increases, it can be seen that the areas where the trajectories diverge growth. Chaos and multifrequency oscillations disappear at sufficiently large positive values of the parameters  $a_1$  and  $a_2$  (Fig. 3b). We see that Neimark-Sacker bifurcation occurs on the border of a stable fixed point region, and the invariant curve is born. In the region of

quasi-periodicity, a fairly wide window of periodic regimes is also observed, to which an attractor in the form of a 39-cycle corresponds.

With a further increase of discretization parameter in Fig. 3c one can see that area of divergence continues to expand, and area with attractors became small (it is necessary to scale the parameter plane again). One can observe many narrow windows of periodic regimes embedded in both the region of quasi-periodicity and chaos. The first such window corresponds to a cycle of period 78. The remaining windows correspond to even longer-period cycles. We can observe transition to chaos and even formation of hyperchaos.

In the system under consideration, by analogy with the continuous model [41, 42, 44, 46], we can introduce an additional parameter  $\Delta$  characterizing the frequency mismatch of the oscillators:

$$\begin{aligned}
x_{n+1} &= x_n - \varepsilon((1 - \Delta)y_n + z_n), \\
y_{n+1} &= y_n + \varepsilon((1 - \Delta)x_n + a_1y_n) + \varepsilon\mu(v_n - y_n), \\
z_{n+1} &= z_n + \varepsilon b + \varepsilon(x_n - r)z_n, \\
u_{n+1} &= u_n - \varepsilon((1 + \Delta)v_n + w_n), \\
v_{n+1} &= v_n + \varepsilon((1 + \Delta)u_n + a_2v_n) + \varepsilon\mu(y_n - v_n), \\
w_{n+1} &= w_n + \varepsilon b + \varepsilon(u_n - r)w_n.
\end{aligned} \tag{5}$$

In the center of Fig. 5 we show the Lyapunov exponents chart of such a system on the plane of control parameters  $(a_1, a_2)$ . The values of the frequency mismatch and the coupling parameter are chosen so that in the system (5) at typical values  $a_1 = a_2 = 0.15$  a three-frequency regime is observed. Let's compare the chart in Fig. 5 with Fig. 3a. It can be seen that the parameter plane has become asymmetric, which is associated with the violation of the symmetry of the system when non-identity is introduced due to the frequency mismatch. The second nuance is the disappearance of the two-frequency region in the area near the diagonal  $a_1 = a_2$  and its replacement by three-frequency regimes. This is also caused by the fact that the subsystems are not identical due to the frequency mismatch. The introduction of a frequency mismatch in its turn leads to a notable system of tongues of resonant invariant curves immersed in the region of three-frequency regimes. Chaos results from the overlap of these tongues.

The periphery of Fig. 5 presents the phase portraits in projection onto the variables of the second oscillator at selected points of the parameter plane. In Fig. 5c one can see the "basic" two-dimensional torus (three-frequency quasi-periodic regime). The rest of the fragments refer to different tongues of two-frequency quasi-periodicity embedded in the three-frequency region.

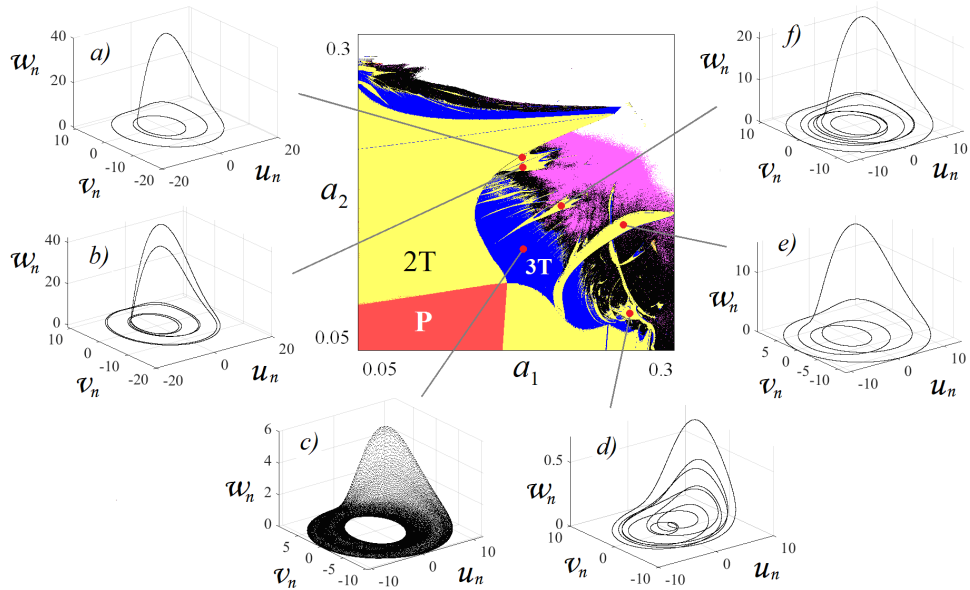


Figure 5: Lyapunov exponents chart of system (5) on the plane of control parameters  $(a_1, a_2)$ ;  $r = 8.5$ ,  $b = 0.4$ ,  $\mu = 0.23$ ,  $\varepsilon = 0.1$ ,  $\Delta = 0.193$ .

Figure 5a shows an invariant curve (two-frequency torus) corresponding to two loops projected onto the horizontal plane  $(v, u)$ . Figure 5b displays a doubling of such a curve. Fig. 5e corresponds to three loops, and Fig. 5d, f - to their large number.

Accounting for an additional frequency parameter makes it possible to study the structure of the parameter plane "the frequency mismatch - coupling parameter  $(\Delta, \mu)$ " for the equal values of control parameters  $a_1 = a_2 = 0.15$  by analogy with the prototype system [44]. Figure 6 shows the corresponding Lyapunov exponents chart (a) and its enlarged fragment (b). It can be seen that a stable fixed point is observed on a large area of chart. Such a regime comes to replace the mode of oscillations death in the prototype continuous system [44]. The mentioned region is surrounded by a domain of two-frequency quasi-periodicity 2T, for which, in contrast to Ref. [44], resonant periodic regimes are not observed. When the coupling decreases, the two-frequency regimes are transformed into three-frequency regimes 3T. A totality of resonant tongues of two-frequency quasi-periodicity is built into 3T area. It is well visualized on the enlarged fragment of the chart in Fig. 6b. As the coupling decreases further, the tongues of the two-frequency quasi-

periodic regimes begin to overlap, and chaos C appears with development to hyperchaos H.

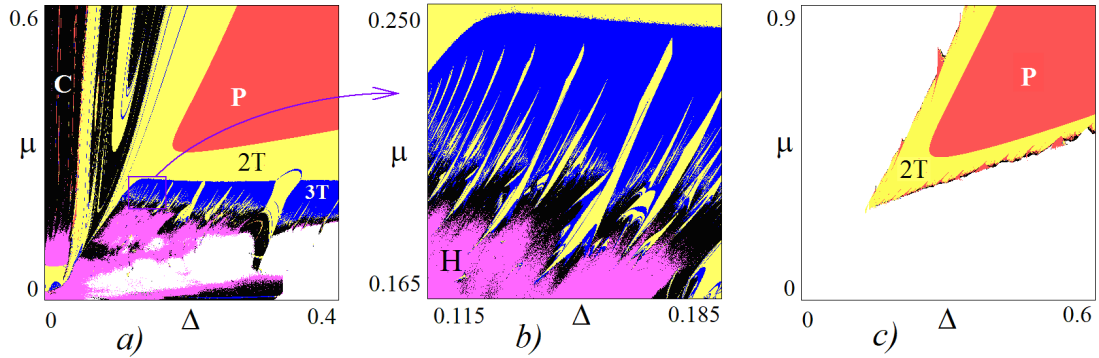


Figure 6: Lyapunov exponents chart of system (5) on the plane “frequency mismatch of oscillators - the coupling parameter” (a) and its enlarged fragment (b);  $r = 8.5$ ,  $a_1 = a_2 = 0.15$ ,  $b = 0.4$ ,  $\varepsilon = 0.1$ . Fragment (c): Lyapunov exponents chart of system (5) for parameters  $r = 8.5$ ,  $a_1 = a_2 = 0.15$ ,  $b = 0.4$ ,  $\varepsilon = 0.16$ .

Let us now increase the discretization parameter  $\varepsilon$ . The corresponding chart for  $\varepsilon = 0.16$  is shown in Fig. 6c. It can be seen that the regimes of three-frequency tori disappear, and the region of trajectory divergence begins to dominate. Along the edges of the two-frequency region, a composition of small tongues of periodic regimes and chaos is observed.

### 2.3 Three coupled discrete oscillators (“chain” case)

Consider now the case of three coupled discrete Rössler oscillators. Such a system is expected to demonstrate nontrivial dynamics, for example, by analogy with the case of three coupled two-dimensional delayed logistic maps [47, 48].

First, let us choose the coupling that corresponds to the chain, when the first oscillator is coupled only with the second one, the second - with the first and third ones, and the third - with the second (scheme of coupling is shown in Fig. 7a). Let us write down the equations of the system by analogy with

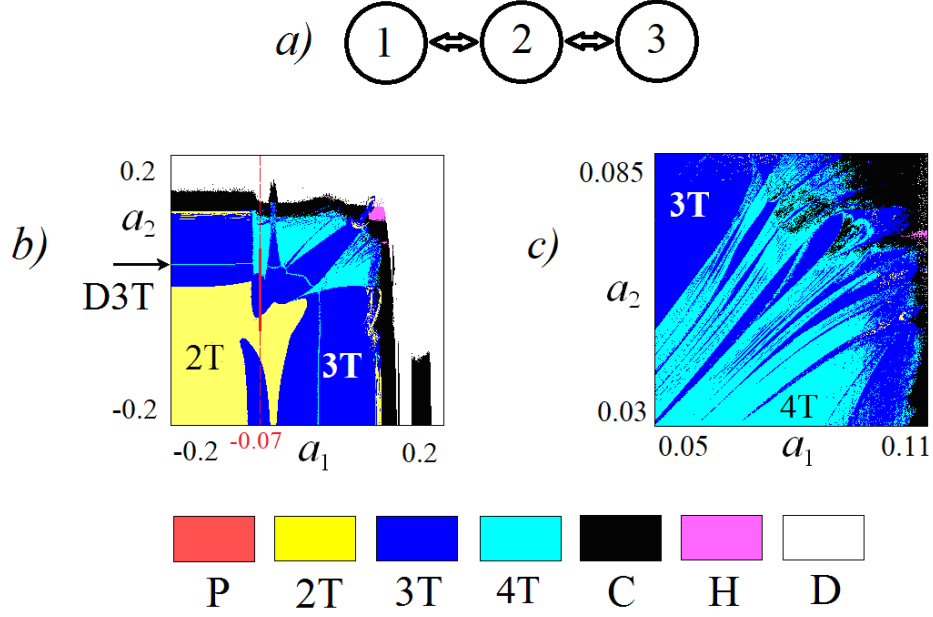


Figure 7: (a) Scheme of three oscillators coupling as a chain. (b) Lyapunov exponents chart of the chain of three coupled oscillators (6) on the plane of the control parameters of the first and second oscillators ( $a_1, a_2$ ). The values of the control parameter of the third oscillator  $a_3 = -0.05$ , the coupling parameter  $\mu = 0.02$ , the remaining parameters  $r = 8.5$ ,  $b = 0.1$ ,  $\varepsilon = 0.1$ ,  $\Delta_1 = \Delta_2 = 0$ . (c) Enlarged fragment of the chart (b)

the prototype continuous system [44]:

$$\begin{aligned}
x_{n+1} &= x_n - \varepsilon(y_n + z_n), \\
y_{n+1} &= y_n + \varepsilon(x_n + a_1 y_n) + \varepsilon\mu(v_n - y_n), \\
z_{n+1} &= z_n + \varepsilon b + \varepsilon(x_n - r)z_n, \\
u_{n+1} &= u_n - \varepsilon((1 - \Delta_1)v_n + w_n), \\
v_{n+1} &= v_n + \varepsilon((1 - \Delta_1)u_n + a_2 v_n) + \varepsilon\mu(y_n + q_n - 2v_n), \\
w_{n+1} &= w_n + \varepsilon b + \varepsilon(u_n - r)w_n, \\
p_{n+1} &= p_n - \varepsilon((1 - \Delta_2)q_n + s_n), \\
q_{n+1} &= q_n + \varepsilon((1 - \Delta_2)p_n + a_3 q_n) + \varepsilon\mu(v_n - q_n), \\
s_{n+1} &= s_n + \varepsilon b + \varepsilon(p_n - r)s_n.
\end{aligned} \tag{6}$$

Here  $\Delta_1$  and  $\Delta_2$  are frequency mismatches of the second and third oscillators

relative to the first. At the beginning by analogy with the case of two oscillators, we present the arrangement of the control parameters plane  $(a_1, a_2)$  for zero frequency mismatches  $\Delta_1 = \Delta_2 = 0$ . The corresponding chart is shown in Figure 7b. The control parameter of the third oscillator is chosen equal to the magnitude  $a_3 = -0.05$ , which, for the given values of the other parameters, corresponds to the quasi-periodic regime in this oscillator in the autonomous case. For three coupled oscillators we again found new type of dynamical regime:

- 4T means an invariant 3D torus - a four-frequency quasi-periodic regime (three zero exponents  $\Lambda_1 = \Lambda_2 = \Lambda_3 = 0$ ,  $\Lambda_{4,5,6,7,8,9} < 0$ ).

First of all, we note the absence of a periodic synchronization regime for all oscillators, which is due to the quasi-periodic dynamics of the third oscillator. The picture is asymmetric compared to Fig. 3a, that is also because of the interaction of the second oscillator with the third one. With an increase in one of the control parameters with a fixed second, and also with an approximate equality of the parameters  $a_1$  and  $a_2$ , three-frequency quasi-periodicity 3T is born from invariant curve 2T. Now, however, regimes of four-frequency quasi-periodicity 4T appear between these regions, for which three Lyapunov exponents are zero  $\Lambda_{1,2,3} = 0$ , and all the rest are negative. A set of resonant tongues of three-frequency quasi-periodicity is built into the region of four-frequency quasi-periodicity, which is illustrated by a zoomed fragment of Lyapunov exponents chart in Fig. 7c. Note that with an increase in the coupling parameter  $\mu$ , this set of tongues becomes more expressed. We also note that similarly with Fig. 3a in the region of three-frequency quasi-periodicity, one can see doubling line D3T.

Let us discuss the mechanism of the emergence of different dimension tori. To do this, we turn to the graphs of the largest Lyapunov exponents depending on the parameter  $a_2$ , plotted along the red line  $a_1 = -0.07$  in Fig. 7b (the thicker section of the red line corresponds to the selected range for the parameter  $a_2$ ). These graphs are shown in Fig. 8. It can be seen that for small values of  $a_2$ , one exponent is zero  $\Lambda_1 = 0$ , and the rest are negative, so that a invariant curve (two-frequency quasi-periodicity) is realized in the system. At the point  $QSN_1$ , the exponent  $\Lambda_2$  also turns to zero, which then remains zero, so that a two-dimensional torus (three-frequency quasi-periodicity) is born. The nature of the behavior of Lyapunov exponents allows, according to the method [49], to identify this transition as a saddle-node bifurcation of invariant curves when a stable invariant curve collides with a saddle invariant curve, as a result of which a two-dimensional torus

is emerged. With the growth of the control parameter  $a_2$ , other exponents show similar behavior. Before the point  $\text{QSN}_2$ , two exponents  $\Lambda_{1,2} = 0$  are equal to zero, and  $\Lambda_{3,4} < 0$ . At the point  $\text{QSN}_2$ , the exponent  $\Lambda_3$  vanishes and then remains zero, so that  $\Lambda_{1,2,3} = 0$ . By the method of [49], we identify this bifurcation as a saddle-node bifurcation of two-dimensional tori.

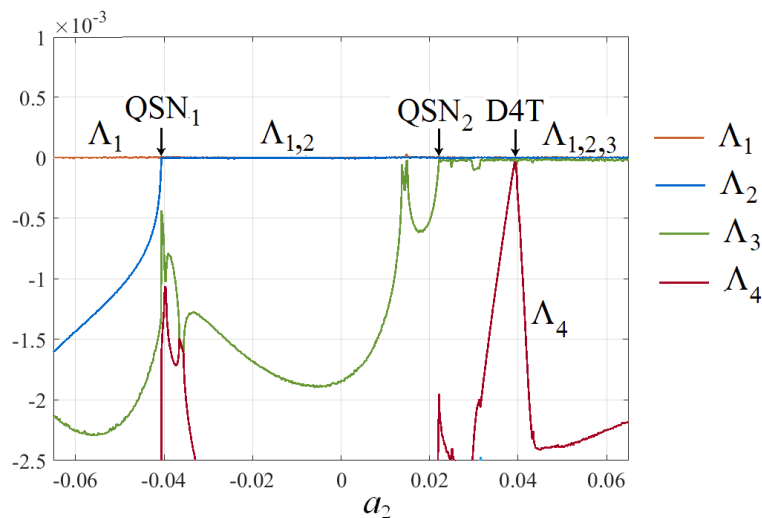


Figure 8: Graphs of the largest Lyapunov exponents depending on the parameter  $a_2$ , other parameters  $r = 8.5$ ,  $b = 0.1$ ,  $\varepsilon = 0.1$ ,  $\mu = 0.02$ ,  $\Delta_1 = \Delta_2 = 0$ ,  $a_1 = -0.07$ ,  $a_3 = -0.05$ .  $\text{QSN}$  are points of saddle-node bifurcations of tori,  $\text{D4T}$  is a point of a four-frequency torus doubling.

The behavior of Lyapunov exponents in Fig. 8 makes it possible to reveal one more tori bifurcation. At point  $\text{D4T}$ , not only the exponents  $\Lambda_{1,2,3}$  are equal to zero, but the fourth exponent  $\Lambda_4$  also vanishes. At the same time, in the vicinity of this point, it remains negative. According to [49], this corresponds to the doubling bifurcation of a three-dimensional torus which corresponds to four-frequency quasi-periodicity. On the chart in Fig. 7b, the line of three-dimensional tori doubling is a continuation of two-dimensional tori doubling line  $\text{D3T}$ .

Figure 9 shows the Fourier spectra for two-, three- and four-frequency quasiperiodicity as an illustration of the different regimes. One can see the structure of the spectra, which is characteristic of quasi-periodic oscillations, and their successive complication with an increase in the number of

incommensurable frequencies. For the simplest two-frequency quasi-periodic regime (an invariant curve in the phase space of map (6)) Fourier spectrum is discrete, it has a main peak and satellite peaks, which corresponds to combinations of two frequency components (Fig. 9a). The transition to three-frequency quasi-periodicity lead to the birth of satellite peaks near each frequency peak of two-frequency quasi-periodicity. In Fig. 9b, we see such a transition, Fourier spectrum has become more complex, near each satellite peak of two-frequency quasi-periodicity the set of new peaks is observed, but it is clear that the spectrum is discrete. Figure 9c shows Fourier spectrum of the four-frequency quasi-periodicity. It can be seen that spectrum has become more complicated (additional satellite peaks were born) and it is close to continuous, but discrete components are preserved.

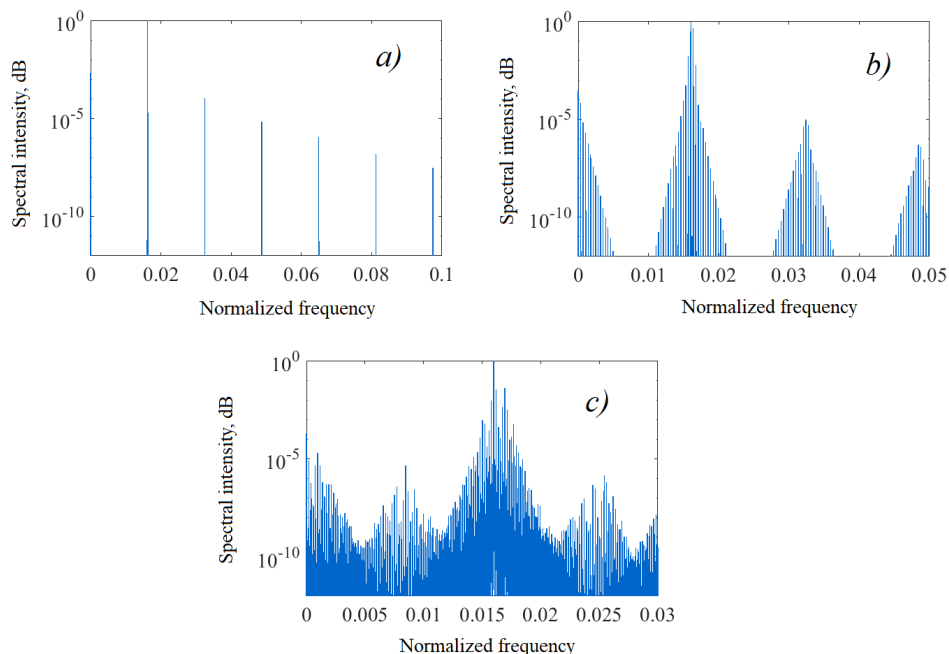


Figure 9: Fourier spectra of chain consisted of three coupled discrete oscillators (6) at  $a_1 = -0.07$  for a two-frequency torus  $a_2 = -0.05$  (a), a three-frequency torus  $a_2 = -0.02$  (b), a four-frequency torus  $a_2 = 0.05$  (c). Other parameters are  $a_3 = -0.05$ ,  $r = 8.5$ ,  $b = 0.1$ ,  $\mu = 0.02$ ,  $\varepsilon = 0.1$ ,  $\Delta_1 = \Delta_2 = 0$ .

Let us now discuss the case of nonzero frequency mismatches of oscillators.

It is convenient to construct the parameter plane of frequency mismatches  $(\Delta_1, \Delta_2)$  (by analogy with the case of a chain of coupled van der Pol oscillators [50] and a flow system of three Rössler oscillators [44]). Figure 10 shows the corresponding Lyapunov exponents chart for  $a_1 = a_2 = a_3 = 0.1$  and  $\varepsilon = 0.02$ ,  $\mu = 0.06$ . It can be seen that two-frequency regimes are observed mainly in a small range of parameters in the vicinity of zero frequency mismatch, when the characteristic frequencies of all oscillators coincide (area in Fig. 10 near point  $\Delta_1 = \Delta_2 = 0$ ).

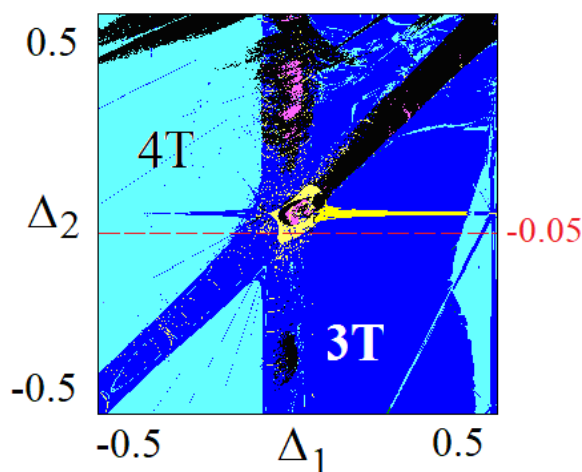


Figure 10: Lyapunov exponents chart of the three coupled in a chain oscillators (6) for the values of the parameters  $r = 8.5$ ,  $b = 0.1$ ,  $a_1 = a_2 = a_3 = 0.1$ ,  $\mu = 0.06$ ,  $\varepsilon = 0.02$ .

On Fig. 11a we present graphs of Lyapunov exponents depending on the frequency mismatch of the central oscillator  $\Delta_1$  and characteristic phase portraits along the red horizontal dotted line  $\Delta_2 = -0.05$  in the Fig. 10. As  $\Delta_1$  increases, four-frequency tori, three-frequency tori, two-frequency tori, and then again three- and four-frequency tori are sequentially observed. The phase portraits evolve accordingly.

Let us now discuss bifurcations of invariant tori. As can be seen from the graphs in Fig. 11a to the left of the QH point, two exponents  $\Lambda_{1,2} = 0$  are zero, and the rest are negative. However, up to the point QH, two of them are equal to each other, i.e.  $\Lambda_3 = \Lambda_4$ . When passing through this point from

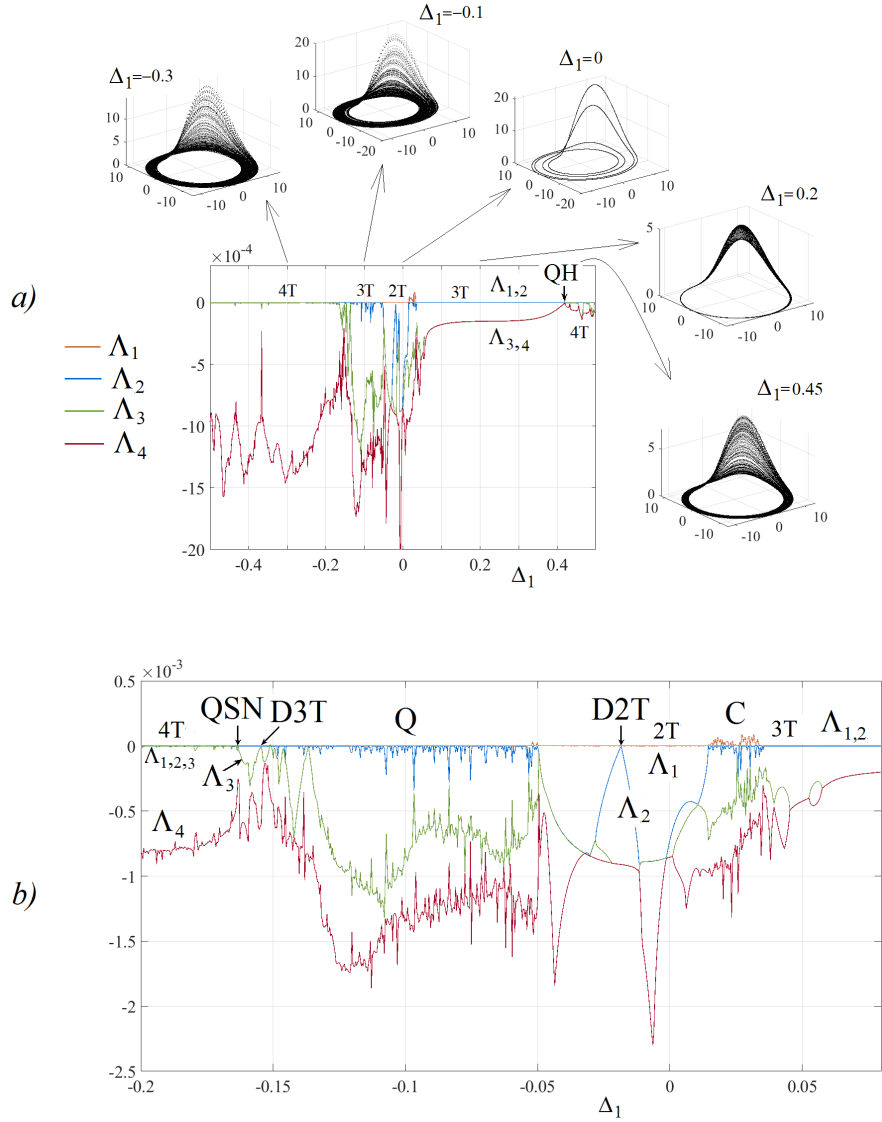


Figure 11: (a): Graphs of Lyapunov exponents and characteristic phase portraits for parameter values corresponding to Fig. 10 and  $\Delta_2 = -0.05$ . QH is the point of quasi-periodic bifurcation of three-frequency tori. (b): Zoomed fragment of graphs of Lyapunov exponents in Fig. 11a.

left to right, the third exponent becomes zero  $\Lambda_3 = 0$ , and the fourth again tend to the negative region  $\Lambda_4 < 0$ . In accordance with [49], a bifurcation of

tori appears different from the one we mentioned above, namely the quasi-periodic Hopf bifurcation QH, when a four-frequency torus is born from a three-frequency one in a soft way. Note that several windows of resonant three-frequency tori are visible to the right of the QH point in the 4T region.

The details of the transition between tori of different dimensions are illustrated in Fig. 11b, which shows an enlarged fragment of Lyapunov exponent graphs from Fig. 11a. This fragment occupies the area of two-frequency tori 2T and bordering areas. At large  $\Delta_1$  in this Figure, a three-torus 3T with  $\Lambda_{1,2} = 0$  is observed. When the parameter  $\Delta_1$  decreases, the torus collapses and a narrow window of chaos C appears. Next, two-torus 2T arises, for which  $\Lambda_1 = 0$ . Inside this region, the point of the two-frequency torus doubling D2T is clearly visible; exactly in this point the second exponent vanishes  $\Lambda_2 = 0$ . Then there is a certain transition region Q, inside which the second exponent oscillates near zero: here the windows of two-frequency and three-frequency tori alternate. At small  $\Delta_1$ , a saddle-node bifurcation of a three-frequency torus occurs at the point QSN, as a result of which a four-torus 4T is born (type of bifurcation is determined by the corresponding behavior of the exponents  $\Lambda_3$  and  $\Lambda_4$ ). Note that the doubling bifurcation point of the three-frequency torus D3T is also well visualized.

## 2.4 Three coupled discrete oscillators ("network" case)

For three oscillators, another type of coupling is also possible, when each oscillator is coupled to each (case of "ring" or "network", schematic representation is shown in Fig. 12a). In this case, the equations of the system have the next form:

$$\begin{aligned}
x_{n+1} &= x_n - \varepsilon(y_n + z_n), \\
y_{n+1} &= y_n + \varepsilon(x_n + a_1 y_n) + \varepsilon\mu(v_n + q_n - 2y_n), \\
z_{n+1} &= z_n + \varepsilon b + \varepsilon(x_n - r)z_n, \\
u_{n+1} &= u_n - \varepsilon((1 - \Delta_1)v_n + w_n), \\
v_{n+1} &= v_n + \varepsilon((1 - \Delta_1)u_n + a_2 v_n) + \varepsilon\mu(y_n + q_n - 2v_n), \\
w_{n+1} &= w_n + \varepsilon b + \varepsilon(u_n - r)w_n, \\
p_{n+1} &= p_n - \varepsilon((1 - \Delta_2)q_n + s_n), \\
q_{n+1} &= q_n + \varepsilon((1 - \Delta_2)p_n + a_3 q_n) + \varepsilon\mu(v_n + y_n - 2q_n), \\
s_{n+1} &= s_n + \varepsilon b + \varepsilon(p_n - r)s_n.
\end{aligned} \tag{7}$$

Figure 12b shows the Lyapunov exponents chart of this system on the plane of the control parameters of the first and second oscillators ( $a_1, a_2$ ) in

the absence of frequency mismatches  $\Delta_1 = \Delta_2 = 0$ . It should be compared with the case of the chain in Figure 7b. It can be seen that the picture for the network and the chain is qualitatively similar. However, for the network, the plane of control parameters becomes symmetric. This is not surprising: for a system in the form of a network, all oscillators are equivalent in the absence of frequency mismatches. That is not so in the case of a chain.

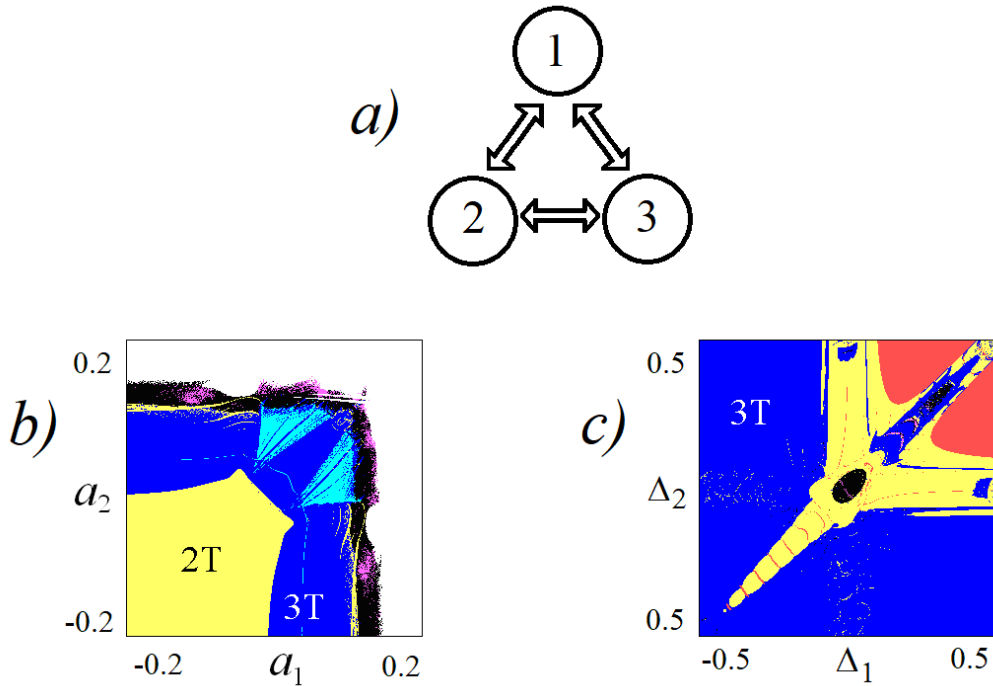


Figure 12: Coupling scheme of three oscillators as a ring, or network (a). Lyapunov exponents charts of a network of three oscillators: (b) on the plane of control parameters for  $\Delta_1 = \Delta_2 = 0$ ,  $a_3 = -0.05$ ,  $\varepsilon = 0.1$ , (c) on the plane of frequency mismatches for  $a_1 = a_2 = a_3 = 0.1$ ,  $\mu = 0.06$ ,  $\varepsilon = 0.02$ . The remaining parameters are  $r = 8.5$ ,  $b = 0.1$ .

This case can also be compared with Fig. 3a, when two identical oscillators interacted. The structure of the chart is very similar, but the basic self-oscillating mode is not a fixed point, but an invariant curve. As the parameters  $a_1$ ,  $a_2$  increase, the birth of a two-frequency torus, its doubling bifurcation and also two symmetrical regions in the form of tongues of a

three-frequency torus are observed. Thus, the picture is completely similar to Fig. 3a, but with an additional frequency component.

Figure 12c presents a chart in the presence of frequency mismatches on the plane  $(\Delta_1, \Delta_2)$ , which should be compared with Figure 10 for the case of a chain. We can also see the availability of symmetry, but in this case three-frequency tori 3T dominate.

### 3 Discrete hyperchaotic Rössler oscillator (Four-dimensional)

The four-dimensional Rössler system with hyperchaos [30,51] has the form

$$\begin{aligned}\dot{x} &= -y - z, \\ \dot{y} &= x + ay + w, \\ \dot{z} &= b + xz, \\ \dot{w} &= -cz + dw.\end{aligned}\tag{8}$$

Here  $a, b, c, d$  are parameters. And accordingly, the discrete system has the next form

$$\begin{aligned}x_{n+1} &= x_n - \varepsilon(y_n + z_n), \\ y_{n+1} &= y_n + \varepsilon(x_n + ay_n + w_n), \\ z_{n+1} &= z_n + \varepsilon(b + x_n z_n), \\ w_{n+1} &= w_n - \varepsilon(cz_n - dw_n).\end{aligned}\tag{9}$$

Figure 13 shows the Lyapunov exponents charts of system (9) for various values of the discretization parameter  $\varepsilon$ . For small values of the parameter  $\varepsilon$ , the structure of the chart is very close to that for the flow system (8) [51], but with the replacement of periodic regimes in the prototype system by two-frequency ones, and two-frequency regimes by three-frequency ones.

The simplest attractor implemented in the map (9) is the invariant curve, which is observed for sufficiently large values of the parameter  $b$ . As the parameter  $b$  decreases, the invariant curve loses stability as a result of the quasi-periodic Hopf bifurcation and a two-dimensional torus is born. (We will explain the type of bifurcation below.) With a further decrease in the parameter  $b$ , the two-dimensional torus is destroyed, and chaos or hyperchaos is observed in the map. The chart also shows that within tongues with an invariant curve, a quasi-periodic Hopf bifurcations can occur with formation of two-dimensional torus on the base of different invariant curves.

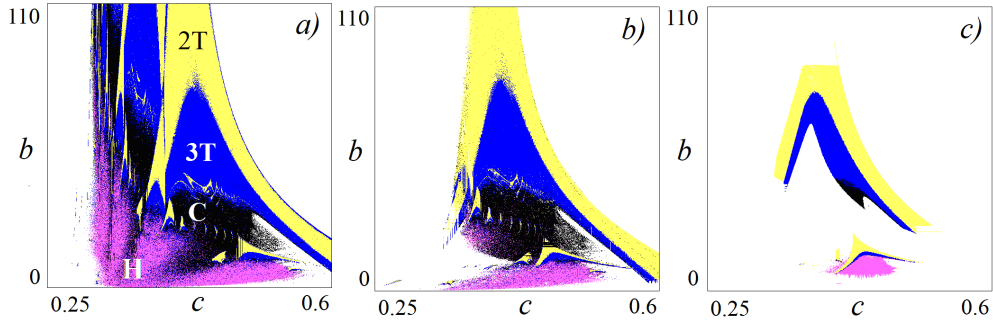


Figure 13: Lyapunov exponents charts of the discrete hyperchaotic Rössler oscillator (9),  $a = 0.25$ ,  $d = 0.05$ , (a)  $\varepsilon = 0.001$ ; (b)  $\varepsilon = 0.01$ ; (c)  $\varepsilon = 0.02$ .

As the discretization parameter  $\varepsilon$  increases, the dynamical regimes disappear at small values of the parameter  $c$ . This feature is due to the fact that as  $c$  decreases, the attractor grows in size and a small increase in the parameter  $\varepsilon$  leads to escape of the trajectories to infinity. In this case, the types of dynamical regimes do not change with an increase in the discretization step.

Consider the features of the phase portraits of map (9) for a mild value of the discretization parameter,  $\varepsilon = 0.01$ . Figure 14 shows graphs of Lyapunov exponents depending on the parameter  $b$  at  $c = 0.4$ , as well as characteristic two-dimensional projections of phase portraits. The graphs of Lyapunov exponents demonstrate the bifurcation of a three-frequency torus birth (QH) and the evolution of chaos. In Fig. 14b, a smooth closed curve is visible, which then undergoes a quasi-periodic Hopf bifurcation (QH) and a stable two-dimensional torus is born (Fig. 14c). The type of bifurcation in accordance with [49] is determined by the character of the behavior of the exponents: up to the bifurcation threshold  $\Lambda_2 = \Lambda_3$ .

It is very difficult to trace the destruction of a two-dimensional torus using phase portraits (Fig. 14d). However, as we can see, the behavior of the map (9) is very close to the behavior of the flow system; accordingly, we can assume an embeddability of the map into the flow. This fact is also confirmed by the presence of a zero Lyapunov exponent for a chaotic attractor; this feature is mandatory for flow systems, while being a special case [13,35] for maps. Then it is possible to analyze the behavior of the system in the Poincaré section. As we noted, it is impossible to strictly implement this procedure for map, since the system is discrete, but we can select a

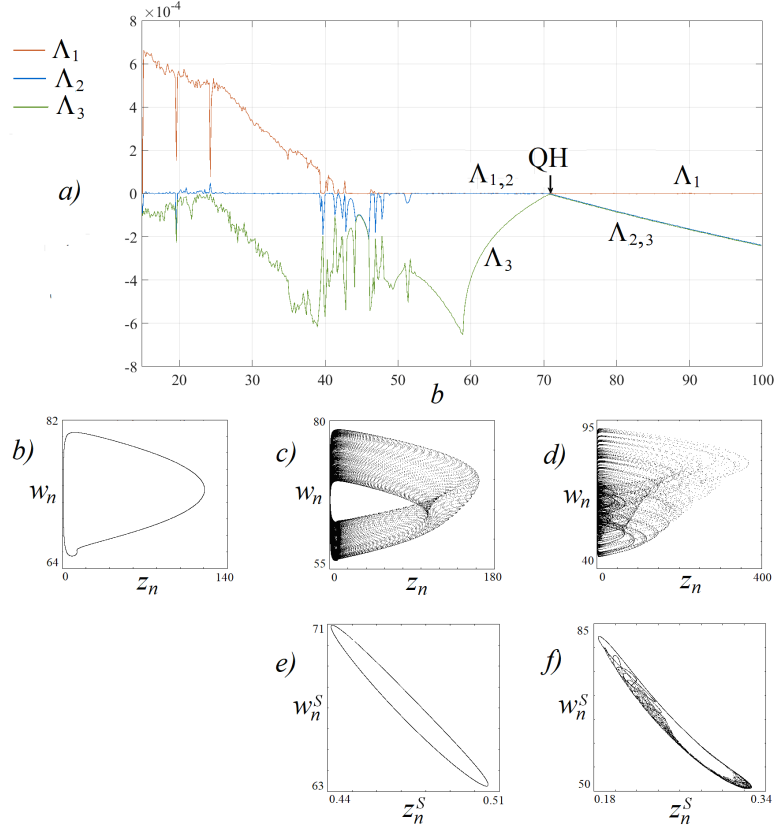


Figure 14: Graphs of Lyapunov exponents at  $c = 0.4$  (a); two-dimensional projections of phase portraits (b, c, d) and their sections (e, f) for the discrete hyperchaotic Rössler oscillator,  $a = 0.25$ ,  $c = 0.4$ ,  $d = 0.05$ ,  $\varepsilon = 0.01$ . (b):  $b = 100$ ; (c), (e):  $b = 65$ ; (d), (f):  $b = 33$ .

certain layer in the phase space so that the points of the map falling into this layer will correspond to the section. As the section plane we chose  $y = 0$  and layer  $2 \cdot 10^{-2}$ . On the graphs we designate the points that fall into the mentioned plane using the superscript "S":  $x_n^S$ ,  $y_n^S$ ,  $z_n^S$ ,  $w_n^S$ . Figures 14e and 14f demonstrate such sections of the phase portraits. It is clearly seen that the section of a two-dimensional torus corresponds to a smooth closed invariant curve (Fig. 14e). The section of the chaotic attractor (Fig. 14f) reveals the complex structure of the attractor, while the basic invariant curve is clearly visible, the destruction of which has occurred. Moreover, this attractor is characterized by one positive Lyapunov exponent.

Similar bifurcations can also occur on the basis of other invariant curves, and hyperchaos can also develop. Figure 15 shows similar illustrations for a two-loop invariant curve at  $c = 0.47$ . On the graph of Lyapunov exponents (Fig. 15a), intervals are clearly visible where one and two largest Lyapunov exponents are equal to zero, which corresponds to attractors in the form of an invariant curve and a two-dimensional torus, respectively. On Fig. 15b and 15c the projections of the attractors are shown, where the two-loop invariant curve and the torus born on its base are clearly visible. On Fig. 15d we present projections of a hyperchaotic attractor.

To analyze the structure of attractors, we also examined their sections presented in Figs.15e-15i. Figures 15e-15f clearly show two smooth invariant curves corresponding to a two-dimensional torus in the full phase space and their destruction. For this case an important feature of the collapse of invariant curves is that the chaotic attractor absorbs an unstable invariant curve corresponding to the base one, thus forming a discrete chaotic Shilnikov attractor [39], which has two-dimensional unstable manifold. On Fig. 15g we demonstrate an example of a two-component Shilnikov discrete attractor that is hyperchaotic. A further decrease in the parameter  $b$  leads to the merging of the attractor components and the development of a more complex hyperchaotic attractor (Fig. 15h,i).

As noted earlier, for these examples, there is a very exact correspondence between the attractors of the flow and discretized models. The chaotic behavior of a discrete Rössler oscillator is very close to a flow system, since the maximum number of Lyapunov exponents is two, while for map the dynamics could be more complex, there could be three exponents. This feature is due to the fact that the attractor of the system is born on the basis of saddle cycles, has a small basin of attraction and is sensitive to changes in parameters and initial conditions. Increasing the discretization parameter and the number of instabilities in the system leads to the destruction of the attractor and the escape of trajectories to infinity.

## 4 Conclusion

Replacing time derivatives with finite differences in the Rössler systems allows us to build an original three- and four-dimensional maps. It is possible to introduce into consideration both an individual such system and two or three coupled maps. The individual map demonstrates the possibility of

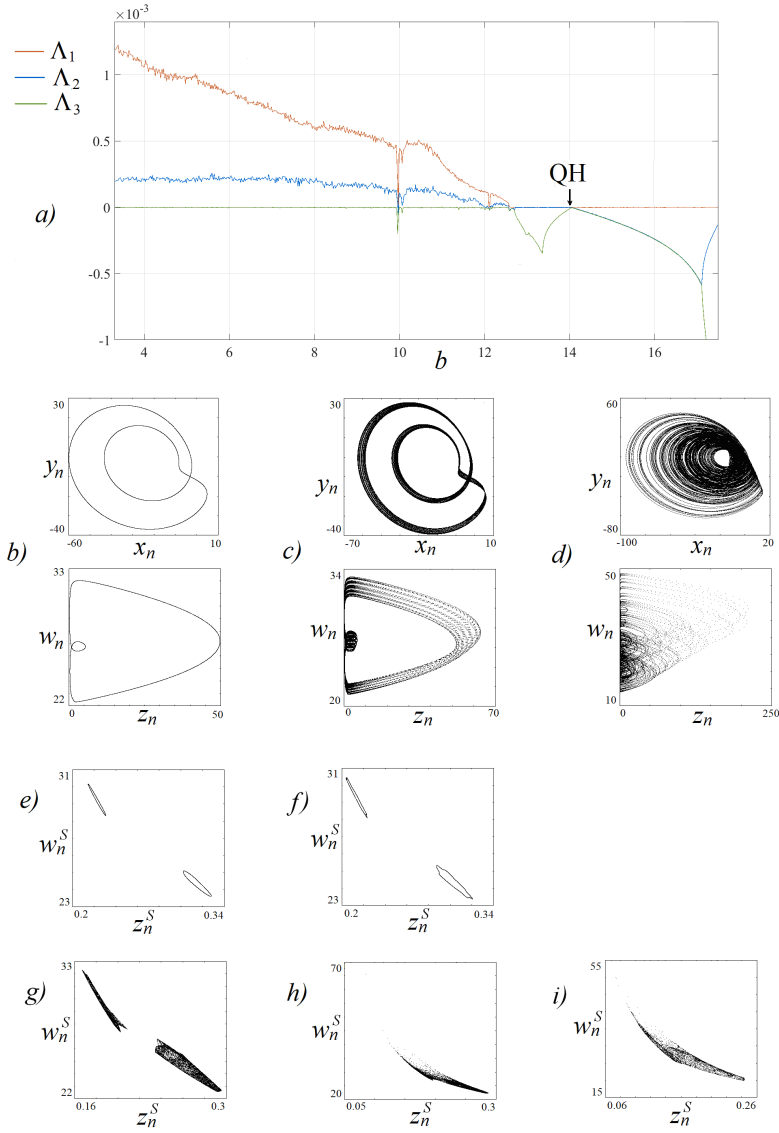


Figure 15: Graphs of Lyapunov exponents at  $c = 0.47$  (a), two-dimensional projections of phase portraits (b, c, d) and their sections (e-i) of the discrete hyperchaotic Rössler oscillator,  $a = 0.25$ ,  $c = 0.4$ ,  $d = 0.05$ ,  $\varepsilon = 0.01$ . (b):  $b = 16.1$ ; (c), (e):  $b = 13.5$ ; (d):  $b = 5.25$ ; (f):  $b = 13$ ; (g):  $b = 11.5$ ; (h):  $b = 11.0$ ; (i):  $b = 8.25$

two-frequency tori (invariant curves) and their doubling. For two and three coupled oscillators, the method of Lyapunov exponents charts is effective, which reveals invariant tori of different dimensions. Two coupled maps exhibit doubling not only of invariant curve, but also of two-dimensional tori. The possibility of frequency mismatch of oscillators is taken into account, which leads to an asymmetry of the picture on the plane of the control parameters. A strongly marked structure of the tongues of resonant invariant curves immersed in the region of three-frequency quasi-periodicity is observed. For the case of three coupled maps, the regions of existence of two-, three- and four-dimensional tori are identified. Analysis of Lyapunov exponents graphs reveals the possibility of quasi-periodic saddle-node bifurcation of two-dimensional invariant tori and quasi-periodic Hopf bifurcation of such tori. Analogies and differences in the structure of Lyapunov exponents charts for the topology of coupling in the form of a chain and a network are discussed.

A discrete version of the Rössler hyperchaotic oscillator is also examined. It is shown that picture of dynamical regimes for a discrete system is close to the original flow system, but with the replacement of periodic regimes by two-frequency, and two-frequency by three-frequency. With an increase in the discretization parameter attractors do not become more complicated, they collapse and the trajectories go to infinity. But for small values of discretization parameter it is possible to obtain discrete chaotic Shilnikov attractors, which corresponds to hyperchaotic dynamical regime.

**Acknowledgments** The study was carried out as part of the State Task of Kotel'nikov's Institute of Radio-Engineering and Electronics of Russian Academy of Sciences.

## References

- [1] Kuznetsov, A.P., Turukina, L.V. & Mosekilde, E. [2001] "Dynamical systems of different classes as models of the kicked nonlinear oscillator," *International Journal of Bifurcation and Chaos* **11**, pp. 1065-1078.
- [2] Zaslavskii, G.M., Roal'd, Z.S., Usikov, D.A. & Chernikov, A.A. [1988] "Minimal chaos, stochastic webs, and structures of quasicrystal symmetry," *Soviet Physics Uspekhi* **31**, pp. 887.

- [3] Morozov, A.D. [1998] *Quasi-conservative systems: cycles, resonances and chaos*, (Series on Nonlinear Science, Series A, Vol. 30, World Scientific, Singapore).
- [4] Zaslavsky, G.M. [2007] *Physics of chaos in Hamiltonian systems*, (Imperial College Press, London).
- [5] Stankevich, N.V., Gonchenko A.S., Popova, E.S. & Gonchenko, S.V. [2023] “Complex dynamics of the simplest neuron model: Singular chaotic Shilnikov attractor as specific oscillatory neuron activity,” *Chaos, Solitons & Fractals* **172**, 113565.
- [6] Li, Y. & Cao, H. [2023] “Bifurcation and comparison of a discrete-time Hindmarsh-Rose model,” *Journal of Applied Analysis and Computation* **13**(1), pp. 34-56.
- [7] Muni, S.S. [2023] “Mode-locked orbits, doubling of invariant curves in discrete Hindmarsh-Rose neuron model,” *Physica Scripta* **98**, 085205.
- [8] Rajagopalan, S., Janakiraman, S. & Rengarajan, A. [2019] “Medical image encryption: Microcontroller and FPGA perspective” in B. Singh, B. Saini, D. Singh, & A. Pandey (Eds.) *Medical Data Security for Bioengineers*, IGI Global (pp. 278-304).
- [9] Rodríguez-Orozco, E., García-Guerrero, E.E., Inzunza-Gonzalez, E., López-Bonilla, O.R., Flores-Vergara, A., Cárdenas-Valdez, J.R. & Tlelo-Cuautle, E. [2018] “FPGA-based chaotic cryptosystem by using voice recognition as access key,” *Electronics* **7**(12), p. 414.
- [10] Khoshsiar Ghaziani, R., Govaerts, W. & Sonck, C. [2011] “Codimension-two bifurcations of fixed points in a class of discrete prey-predator systems,” *Discrete Dynamics in Nature and Society* **2011**, Article ID 862494, 27 pages.
- [11] Andrecut, M. & Kauffman, S.A. [2007] “Chaos in a discrete model of a two-gene system,” *Physics Letters A* **367**, pp. 281-287.
- [12] de Souza, S.L.T., Lima, A.A., Caldas, I.L, Medrano-T., R.O., Guimarães-Filho, Z.O. [2012] “Self-similarities of periodic structures for a discrete model of a two-gene system,” *Physics Letters A* **376**, pp. 1290-1294.

- [13] Popova, E.S., Stankevich, N.V., Kuznetsov, A.P. [2020] “Cascade of invariant curve doubling bifurcations and quasi-periodic Hénon attractor in the discrete Lorenz-84 model,” *Izvestiya of Saratov University. Physics* **20**, pp. 222-232 (in Russian).
- [14] Zaitsev, V.V. [2019] “Physically reasonable time sampling in mathematical models of generators of regular and chaotic oscillations,” *Physics of Wave Processes and Radio Systems* **22**, pp. 44-48 (in Russian).
- [15] Kuznetsov A.P. & Sedova Y.V. [2016] “The simplest map with three-frequency quasi-periodicity and quasi-periodic bifurcations,” *International Journal of Bifurcation and Chaos* **26**, 1630019.
- [16] Zaitsev, V.V. [2017] “The discrete van der Pol oscillator: finite differences and slow amplitudes,” *Izvestiya VUZ. Applied Nonlinear Dynamics* **25**, pp. 70-78 (in Russian).
- [17] Rybalova, E., Muni, S., Strelkova G. [2023] “Transition from chimera/solitary states to traveling waves,” *Chaos* **33**, 033104.
- [18] Kuznetsov, A.P., Savin, A.V., Sedova, Yu.V., Turukina, L.V. [2012] *Bifurcations of maps*, (Saratov: Publishing center "Nauka") (in Russian).
- [19] Arrowsmith, D.K., Cartwright, J.H., Lansbury, A.N., & Place, C.M. [1993] “The Bogdanov map: Bifurcations, mode locking, and chaos in a dissipative system,” *International Journal of Bifurcation and Chaos* **3**, pp. 803-842.
- [20] Kuznetsov, A.P., Savin, A.V., Sedova, Y.V. [2009] “Bogdanov-Takens bifurcation: from flows to discrete systems,” *Izvestiya VUZ. Applied Nonlinear Dynamics* **17**, pp. 139-158 (in Russian).
- [21] Maistrenko, V., Vasylenko, A., Maistrenko, Y., Mosekilde, E. [2008] “Phase chaos and multistability in the discrete Kuramoto model,” *Nonlinear Oscillations* **11**, pp. 229-241.
- [22] Maistrenko, V., Vasylenko, A., Maistrenko, Y., Mosekilde, E. [2010] “Phase chaos in the discrete Kuramoto model,” *International Journal of Bifurcation and Chaos* **20**, pp. 1811-1823.

- [23] Barlev, G., Girvan, M. & Ott, E. [2010] “Map model for synchronization of systems of many coupled oscillators,” *Chaos: An Interdisciplinary Journal of Nonlinear Science* **20**, 023109.
- [24] Kuznetsov, A.P. & Sedova, Y.V. [2014] “Low-dimensional discrete Kuramoto model: Hierarchy of multifrequency quasiperiodicity regimes,” *International Journal of Bifurcation and Chaos* **24**, 1430022.
- [25] Shim, W. [2020] “On the generic complete synchronization of the discrete Kuramoto model,” *Kinetic & Related Models* **13**, pp. 979.
- [26] Rössler, O.E. [1976] “An equation for continuous chaos,” *Physics Letters A* **57**, pp. 397-398.
- [27] Zhao, X., Liu, J., Chen, G., Chai, L. & Wang, D. [2022] “Dynamics and synchronization of complex-valued ring networks,” *International Journal of Bifurcation and Chaos* **32(05)**, 2230011.
- [28] Zhang, X., Liu, J., Wang, D. & Liu, H. [2023] “Geometric control and synchronization of a complex-valued laser chain network,” *Nonlinear Dynamics* **111(7)**, pp. 6395-6410.
- [29] Adilova, A.B., Kuznetsov, A.P. & Savin, A.V. [2013] “Complex dynamics in the system of two coupled discrete Rossler oscillators,” *Izvestiya VUZ. Applied Nonlinear Dynamics* **21**, pp. 108-119 (in Russian).
- [30] Rossler, O.E. [1979] “An equation for hyperchaos,” *Physics Letters A* **71**, pp. 155-157.
- [31] Benettin, G., Galgani, L., Giorgilli, A. & Strelcyn, J.-M. [1980] “Lyapunov characteristic exponents for smooth dynamical systems and for hamiltonian systems; a method for computing all of them. part 1: Theory,” *Meccanica* **15(1)**, pp. 9-20.
- [32] Kaneko K. [1983] “Doubling of torus,” *Progress of Theoretical Physics* **69**, pp. 1806-1810.
- [33] Kaneko K. [1984] “Oscillation and doubling of torus,” *Progress of Theoretical Physics* **72**, pp. 202-215.
- [34] Kuznetsov, Yu.A. & Meijer, H.G.E. [2019] *Numerical bifurcation analysis of maps: from theory to software*, (Cambridge University Press).

- [35] Gonchenko, S.V., Ovsyannikov, I.I., Simó, C. & Turaev, D.V. [2005] “Three-dimensional Hénon-like maps and wild Lorenz-like attractors,” *International Journal of Bifurcation and Chaos* **15**, pp. 3493-3508.
- [36] Gonchenko, A. S., Gonchenko, S. V. & Shilnikov, L. P., [2012] “Towards scenarios of chaos appearance in three-dimensional maps,” *Russian Journal of Nonlinear Dynamics* **8**, pp. 3-28 (in Russian).
- [37] Gonchenko, S., Gonchenko, A., Kazakov, A., & Samylyna, E. [2021] “On discrete Lorenz-like attractors,” *Chaos: An Interdisciplinary Journal of Nonlinear Science* **31**, 023117.
- [38] Richter, H. [2008] “On a family of maps with multiple chaotic attractors,” *Chaos, Solitons & Fractals* **36**, pp. 559-571.
- [39] Bakhanova, Y.V., Gonchenko, S.V., Gonchenko, A.S., Kazakov, A.O. & Samylyna, E.A. [2022] “On Shilnikov attractors of three-dimensional flows and maps,” *Journal of Difference Equations and Applications*. DOI:10.1080/10236198.2022.2063051
- [40] Hampton, A. E. & Meiss, J.D. [2022] “The three-dimensional generalized Hénon map: Bifurcations and attractors,” *Chaos: An Interdisciplinary Journal of Nonlinear Science* **32**, 113127.
- [41] Osipov, G.V., Pikovsky, A.S., Rosenblum, M.G. & Kurths, J. [1997] “Phase synchronization effects in a lattice of nonidentical Rössler oscillators,” *Physical Review E* **55**, pp. 2353-2361.
- [42] Osipov, G.V., Hu, B., Zhou, C., Ivanchenko, M. V. & Kurths, J. [2003] “Three types of transitions to phase synchronization in coupled chaotic oscillators,” *Physical Review Letters* **91**, 024101.
- [43] Kuznetsov A. P. & Paksjutov V. I.[2006] “Dynamics of two nonidentical coupled self-sustained systems with period doublings on the example of Rossler oscillators,” *Izvestiya VUZ. Applied Nonlinear Dynamics* **14**, pp. 3-15 (in Russian).
- [44] Kuznetsov, A.P., Migunova, N.A., Sataev, I.R., Sedova, Y.V. & Turukina, L.V. [2015] “From chaos to quasi-periodicity,” *Regular and Chaotic Dynamics* **20**, pp. 189-204.

- [45] Stankevich, N.V., Kuznetsov, A.P., Popova, E.S., & Seleznev, E.P. [2017] “Experimental diagnostics of multi-frequency quasiperiodic oscillations,” *Communications in Nonlinear Science and Numerical Simulation* **43**, pp. 200-210.
- [46] Pikovsky, A., Rosenblum, M. & Kurths, J. [2001] *Synchronization: A universal concept in nonlinear science*, (Cambridge University Press).
- [47] Hidaka, S., Inaba, N., Kamiyama, K., Sekikawa, M. & Endo, T. [2015] “Bifurcation structure of an invariant three-torus and its computational sensitivity generated in a three-coupled delayed logistic map,” *Nonlinear Theory and Its Applications, IEICE* **6**, pp. 433-442.
- [48] Hidaka, S., Inaba, N., Sekikawa, M. & Endo, T. [2015] “Bifurcation analysis of four-frequency quasi-periodic oscillations in a three-coupled delayed logistic map,” *Physics Letters A* **379**, pp. 664-668.
- [49] Broer, H., Simó, C. & Vitolo, R. [2011] “Quasi-periodic bifurcations of invariant circles in low-dimensional dissipative dynamical systems,” *Regular and Chaotic Dynamics* **16**, pp. 154-184.
- [50] Emelianova, Y.P., Kuznetsov, A.P., Turukina, L.V., Sataev, I.R. & Chernyshov, N.Y. [2014] “A structure of the oscillation frequencies parameter space for the system of dissipatively coupled oscillators,” *Communications in Nonlinear Science and Numerical Simulation* **19**, pp. 1203-1212.
- [51] Stankevich, N., Kazakov, A. & Gonchenko, S. [2020] “Scenarios of hyperchaos occurrence in 4D Rössler system ,” *Chaos: An Interdisciplinary Journal of Nonlinear Science* **30**, 123129.